Carbohydrate Polymers 202 (2018) 404–408

Contents lists available at ScienceDirect

Carbohydrate Polymers

journal homepage: www.elsevier.com/locate/carbpol

Water dynamics in silanized hydroxypropyl methylcellulose based hydrogels designed for tissue engineering

N. Buchtová[a], A. D'Orlando[a], P. Judeinstein[b,c], O. Chauvet[a], P. Weiss[d], J. Le Bideau[a,*]

[a] Institut des Matériaux Jean Rouxel (IMN), Université de Nantes, CNRS UMR 6502, 2 rue de la Houssinière B.P. 32229, 44322 Nantes Cedex 3, France
[b] Laboratoire Léon Brillouin, CEA-CNRS UMR 12, CEA Saclay, Université Paris-Saclay, 91191 Gif sur Yvette Cedex, France
[c] Laboratoire de Physique des Solides, UMR 8502 CNRS-Université Paris Sud, Université Paris-Saclay, 91405 Orsay Cedex, France
[d] Regenerative Medicine and Skeleton (RMeS) laboratory, INSERM, Université de Nantes UMR_S 1229, Centre Hospitalier Universitaire de Nantes, Hôtel-Dieu 1 place Alexis Ricordeau B.P. 84215, 44042 Nantes Cedex 1, France

ARTICLE INFO

Keywords:
Hydrogel
Cellulose
Water dynamics
Confinement
Interface

ABSTRACT

Silanized hydroxypropyl methylcellulose based hydrogels were developed for cartilage and intervertebral disc tissue engineering. Herein, study of dynamics of confined water showed two different populations, identified as hydration and bulk-like water. The diffusion coefficient showed that bulk-like water diffuses over distances ~10 µm without being affected by the hydrogel matrix. Addition of silica nanofibers leads to improved mechanical properties and enhanced diffusion coefficient. Good diffusion within hydrogels is essential for the application.

1. Introduction

Hydrogels are becoming increasingly important biomaterials because of their excellent biocompatibility and stimuli responsive characteristics. They are made of cross-linked molecules forming a three-dimensional network highly swollen by an aqueous medium. From a macroscopic point of view, hydrogels behave like solids: they can be shaped like solids and do not flow like liquids. Simultaneously, they present diffusive properties of real solutions with diffusion coefficients depending on the network (Adam et al., 1996). Therefore, hydrogels can be used for many applications, mostly in the biomedical field, such as contact lenses, drug delivery, superabsorbent etc. (Calvert, 2009; Deligkaris, Tadele, Olthuis, & van den Berg, 2010; Drury & Mooney, 2003; Hendrickson & Andrew Lyon, 2009; Satarkar, Biswal, & Hilt, 2010; Slaughter, Khurshid, Fisher, Khademhosseini, & Peppas, 2009; Van Vlierberghe, Dubruel, & Schacht, 2011; Wichterle & Lim, 1960). Among this, composite hydrogels are developed for tissue engineering. Indeed, their hydrated nature is close to that of extracellular matrix, their porosity has a significant role in oxygen and nutrients diffusion and they respond to ambient stimuli, making them effective to replace defective tissue (Asadi et al., 2018; Balagangadharan, Dhivya, & Selvamurugan, 2017; Bourges, Weiss, Daculsi, & Legeay, 2002; Buchtová et al., 2013; Jaikumar et al., 2015; Yu, Bao, Shi, Yang, & Yang, 2017).

Nevertheless, although a high water content is desired, it is also at the origin of the hydrogels' poor mechanical properties, limiting their applications (Anseth, Bowman, & Brannon-Peppas, 1996). The reinforcement of these mechanical properties was thus required. It is a fundamental challenge, motivated by the numerous future applications of toughened hydrogels (Chau et al., 2016; Gaharwar, Peppas, & Khademhosseini, 2014; Shapiro & Oyen, 2013; Yang, Wang, Yang, Shen, & Wu, 2016). New composites have been developed, using for instance chitosan nanofibers or graphene, leading to more compact microstructures and high mechanical strength (Balagangadharan et al., 2017; Yu et al., 2017). We have also proposed to reach such a mechanical reinforcement with colloidal silica nanofibers, thanks to their diameter and form factor close to 50 nm and 20 respectively, allowing their percolation with low charge level (Buchtová et al., 2013; Nojoomi, Tamjid, Simchi, Bonakdar, & Stroeve, 2017). Such colloidal silica were showed to be essentially nontoxic (Zhang et al., 2012). Since these nanocomposites hydrogels were validated for tissue engineering and are gaining consideration (Buchtová et al., 2013; Henry, Clouet, Le Bideau, Le Visage, & Guicheux, 2018), it remains mandatory to decipher the dynamics of the confined water. Since in the native tissues the nutriments are delivered to cells by simple diffusive processes, further application in cartilage and intervertebral disc tissue engineering needs understanding of the morphology of the hydrogels, and of the dynamics of confined water. The water confined within hydrogels exhibits physico-chemical characteristics which are different from classical bulk water. The dynamical behaviour of confined water is closely associated

* Corresponding author.
E-mail address: Jean.LeBideau@cnrs-imn.fr (J. Le Bideau).

https://doi.org/10.1016/j.carbpol.2018.08.143
Received 16 July 2018; Received in revised form 31 August 2018; Accepted 31 August 2018
Available online 05 September 2018
0144-8617/

with the hydrogel's macromolecular network structure, and it depends on each given structure features (Caccavo, Cascone, Lamberti, & Barba, 2018). Numerous researchers have already used experimental techniques such as Nuclear Magnetic Resonance (NMR) and Differential Scanning Calorimetry (DSC) on several kinds of hydrogels to obtain insights on the confined water (Lang, Jiang, Li, & Zheng, 2008; Numata, Katashima, & Sakai, 2011; Sakai, Kuroki, & Satoh, 2008; Yoshida, Hatakeyama, & Hatakeyama, 1993). According to these results, the water in hydrogels can be generally classified according to three types of physical behaviour: (*i*) free (or bulk-like water) which can undergo liquid-to-solid transition at temperatures within usual ranges, and interfacial (bound) water that can be divided into (*ii*) non-freezing water and (*iii*) water which can freeze below or above regular temperature. The observability of these three water types is dependent on the hydrogel's matrix and its hydration level. Conversely, the physical state of confined water should provide useful information on the morphology and physical behaviour of hydrogels. We focus herein on a detailed description of water behaviour inside silanized hydroxypropyl methylcellulose (Si-HPMC) based hydrogels reinforced with mesoporous silica nanofibers (NFs).

2. Material and methods

2.1. Materials

Silanized hydroxypropyl methylcellulose (Si-HPMC) was prepared using 3-glycidoxypropyl trimethoxysilane (GPTMS, ≥98%, Sigma Aldrich, Germany) and hydroxypropyl methylcellulose (HPMC) with hydroxypropoxyl content 9.5% and methoxyl content 28.3% (E4M, Methocel®, Colorcon, The Dow Chemical CompanyTM, UK) according to the procedure described elsewhere (Bourges et al., 2002). The final silicon content in Si-HPMC was 0.7 wt%. Silica nanofibers (NFs) were obtained by one-pot synthesis as reported previously (Rambaud, Vallé, Thibaud, Julián-López, & Sanchez, 2009). All the other reagents were of analytical grade.

2.2. Hydrogel synthesis

The synthesis of pristine Si-HPMC based hydrogel and corresponding Si-HPMC hydrogels reinforced with silica NFs have already been reported elsewhere (Buchtová et al., 2013). Briefly, to prepare such hydrogels the Si-HPMC polymer is dissolved in basic aqueous solution; then 1 vol of this solution is mixed with 0.5 vol of an acidic buffer solution (BS) by means of two interconnected luer-lock syringes. For silica NFs reinforced hydrogels, the desired amount of NFs is dispersed within BS via ultrasonication prior to its blending with the polymer solution. The final precursor solutions of hydrogels or reinforced hydrogels, which are injectable within the first ~10 min, are injected into plastic moulds and kept at room temperature in humid atmosphere (~80% RH) for 2 weeks to complete the polycondensation process.

2.3. Scanning Electron Microscopy in cryogenic mode (cryo-SEM)

Cryo-SEM was performed on Zeiss EVO LS10 microscope at −130 °C and at approx. 10^{-4} Pa with acceleration voltage of 7 kV. Prior any observation, each equilibrated swollen hydrogel was frozen in slush nitrogen and then quickly introduced into the microscope chamber. The sample's surface was cut off, slightly freeze-dried and gold-sputtered directly inside the microscope.

2.4. Differential Scanning Calorimetry (DSC)

DSC thermograms were obtained on Q200 DSC TA Instruments machine. Hydrogels and bulk aqueous solution of the same composition as inside the hydrogels were sealed in aluminum crucibles and rapidly cooled to −50 °C at a heating rate of approx. 40 °C min^{-1}. Then, 10 cycles from −50 to + 40 °C and back were realized with 5 °C min^{-1} speed. The melting temperatures and the corresponding enthalpies were determined for each sample as average values over 10 heating cycles.

2.5. Nuclear Magnetic Resonance (NMR) cryoporometry

NMR cryoporometry measurements were carried out on Bruker AVANCE 400 MHz NMR spectrometer using a 4 mm QXO probe. Hydrogels were prepared in deuterated water and cooled to 220 K within several hours. They were then gradually heated up to 315 K by 5 K steps and equilibration time of 20 min before starting NMR signal acquisition (temperature stability of ± 0.2 K). The NMR signal of both ^{1}H and ^{2}H was recorded at each temperature point across the process of heating. Temperature calibration was done before each set of measurements using a reference methanol sample.

2.6. Pulsed-Gradient Spin-Echo NMR (PGSE)

PGSE-NMR experiments were realized at 300 K on Bruker AVANCE 400 MHz NMR spectrometer equipped with a 5 mm BBOxyz probe. The diffusion coefficients were determined from the classical Stejskal-Tanner equation(Stejskal & Tanner, 1965):

$$\ln(I/I_0) = -DG^2\gamma^2\delta^2(\Delta - \delta/3) \quad (1)$$

where G is the magnitude of the two gradient pulses applied, δ is their duration and Δ is the time interval between them, γ is the gyromagnetic ratio of the nucleus under study and I and I_0 are the integrated intensities of the signals obtained, respectively, with and without gradient pulses. Here, the magnitude of the pulsed field gradient was varied between 0.674 and 32.030 G cm^{-1} in 16 steps. The pulse duration was fixed to 2.5 ms and two experiments were performed with Δ = 50 ms and Δ = 200 ms in order to check that no convection effects occur in the samples, neither restricted diffusion phenomenon. The gyromagnetic ration of hydrogen $\gamma_H = 267.5 \times 10^6$ rad s^{-1}T^{-1}.

3. Results and discussion

3.1. Scanning electron microscopy analysis

Images of the 2 week-old Si-HPMC hydrogel monoliths containing 0 and 3 wt% of silica NFs are shown in the upper left inserts in Fig. 1a and b, resp. As can be seen, the pristine hydrogel, which contains 98 wt% of aqueous solution and only 2 wt% of chemically cross-linked Si-HPMC matrix, is self-standing, completely transparent and colorless. After the addition of 3 wt% of silica NFs, the Si-HPMC hydrogel monolith becomes opaque and whitish. Simultaneously, the compressive modulus of such hydrogels is enhanced as previously reported.(Buchtová et al., 2013) It is important to note that even if all the Si-HPMC based hydrogels contain 98 wt% of confined water, there is no water leaching out even upon compression.

To obtain information about the water-matrix arrangement inside Si-HPMC hydrogels, scanning electron microscopy in cryogenic mode (cryo-SEM) was performed. The fast sample freezing in slush nitrogen (Apkarian & Wright, 2005; Baker, Denton, & Herr, 2013; Sansinena, Santos, Zaritzky, & Chirife, 2012) used to prepare the sample should preserve the morphology of highly hydrated samples. However, it is known that even such fast freezing method leads to a certain deformation of hydrogel's morphology (Efthymiou, Williams, & McGrath, 2017; Aston, Sewell, Klein, Lawrie, & Grøndahl, 2016). Fig. 1a shows the morphology of the pristine Si-HPMC hydrogel. It is similar to morphologies observed typically on freeze-dried hydrogels. A highly porous structure with pore size distribution ranging from 1 μm to several tens of microns can be observed. The pore walls' thickness is about 100 nm, as shown in the upper right insert in Fig. 1a: they are formed

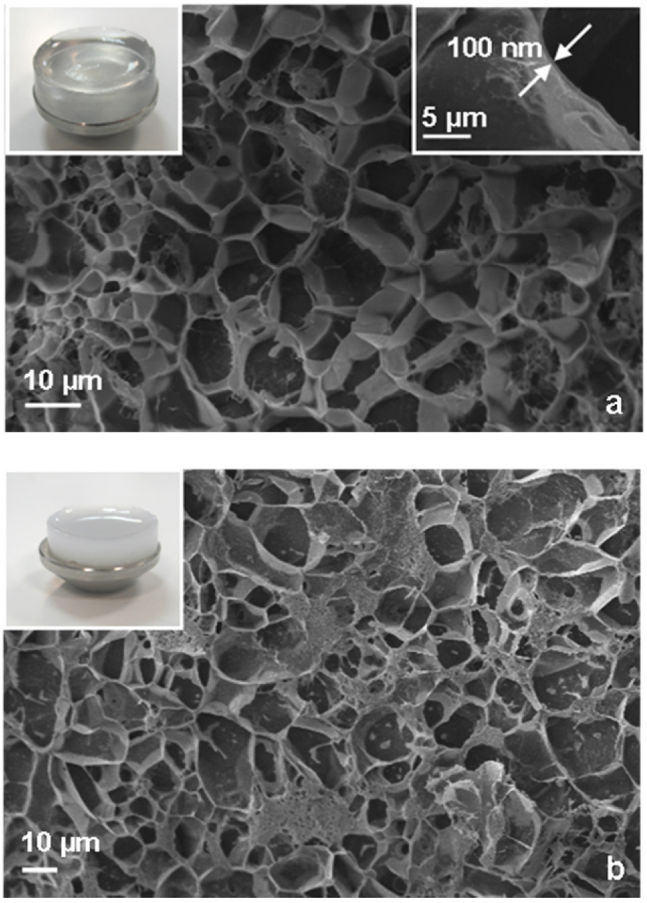

Fig. 1. Cryo-SEM images of (a) Si-HPMC hydrogel and (b) Si-HPMC + 3 wt% NFs hydrogel; inserts: the hydrogel monoliths and the pore wall thickness.

by the polycondensed Si-HPMC polymer chains. The addition of 3 wt% of silica NFs to a Si-HPMC hydrogel does not modify steeply the pore size distribution as can be observed in Fig. 1b. The pores remain micrometer-sized and the pore wall thickness is still around 100 nm. It is worth noting that the NFs cannot be seen using this magnification. The silica nanofibers are well dispersed within all the hydrogel volume and are chemically cross-linked with Si-HPMC polymer to form a hybrid silica-polymer network as already evidenced in our previous work. (Buchtová et al., 2013) Thus, inside both hydrogels all the quantity of water (98 wt%) is confined and retained by the porosity made up of polycondensed Si-HPMC or Si-HPMC polycondensed with silica NFs.

3.2. DSC heating studies

DSC heating thermograms are presented in Fig. 2. The melting temperatures as well as the corresponding enthalpies are also indicated for each melting peak in Fig. 2. It is worth to point out that the aqueous solution, bulk or confined inside each hydrogel, includes salts necessary for hydrogels' synthesis. All the three samples melt at approximatively the same temperature. However, the melting enthalpies of both Si-HPMC and reinforced Si-HPMC hydrogels (228.3 and 238.0 J g^{-1} *resp.*) are lower than the melting enthalpy of the bulk aqueous solution (283.7 J g^{-1}). These results indicate that only ~74 wt% of water inside the pristine Si-HPMC hydrogel and ~84 wt% of water confined in reinforced Si-HPMC hydrogel exhibit solid-to-liquid phase transition in the temperature range explored here (*i.e.* from −50 °C to 40 °C). The remaining amounts of water, approximatively 26 and 16 wt% without and with silica NFs *resp.*, do not undergo any phase change until at least −50 °C. DSC shows thus that the Si-HPMC based hydrogels contain confined water with two different kinds of physical behaviour. Their

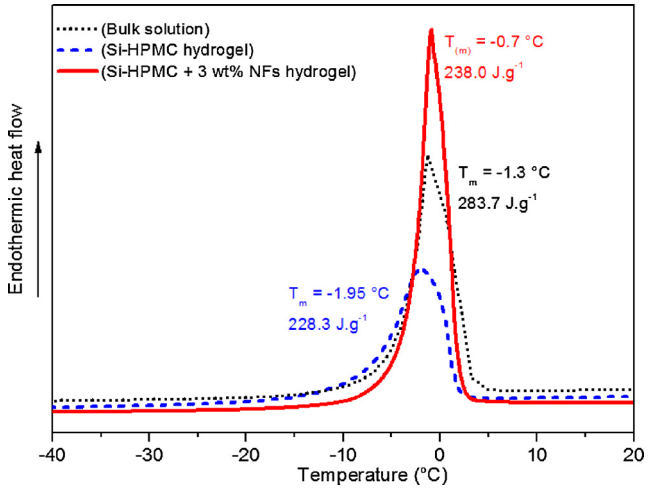

Fig. 2. DSC melting peaks of the bulk solution of the same composition as inside the Si-HPMC based hydrogels, and the pristine and silica NFs reinforced Si-HPMC hydrogels. The melting temperatures (Tm) as well as the enthalpy of melting are indicated for each sample.

amounts vary depending on the presence of silica NFs. Generally, the confined water that undergoes a phase transition at temperatures close to that of the bulk water is named free or bulk-like water. Oppositely, the water whose phase change happens at very different temperatures is interfacial or hydration water (Jhon & Andrade, 1973; Li, Cui, Xiao, & Liao, 2008; Ostrowska-Czubenko & Gierszewska-Drużyńska, 2009; Qu, Wirsén, & Albertsson, 2000; Sekine & Ikeda-Fukazawa, 2009). In conclusion, the water confined in Si-HPMC based hydrogels is composed of approx. 74 wt% of bulk-like water (84 wt% with 3 wt% of silica NFs) and 26 wt% of hydration water (16 wt% with 3 wt% NFs hydrogel). The latter is presumably situated at the interfaces with the hydrophilic hydrogel matrix where it may interacts via hydrogen bonding with the Si-HPMC polymer or silica NFs. Consequently, the behaviour of hydration water is modified as referred to the bulk-like water.

The hydration water forms a physical transition layer between the pore wall of the hydrogel matrix and the bulk-like water which is located far from the interfaces. The amounts of hydration water present in Si-HPMC based hydrogel are similar to results already reported, like for example in chitosan based hydrogels where the quantity of hydration water reach 28 wt% (Qu et al., 2000).

3.3. NMR cryoporometry and PGSE investigations

NMR cryoporometry (Petrov & Furó, 2009; Rault, Neffati, & Judeinstein, 2003) was used to investigate the polymer and water dynamics as a function of temperature. This method allows to quantify the amount of melted (bulk like) liquid. For this purpose, the hydrogel samples were prepared in deuterated water in order to discern the NMR signal of the Si-HPMC matrix (protonated) from the signal given by the confined water (deuterated). Thus in Fig. 3a, the ^{2}H signal area corresponds to the water dynamics, and starting from lower temperatures, it is interesting to note that the signals areas remain substantial below the phase transition temperature (~0 °C). This evidences the existence of water dynamics even at -60 °C, the lower temperature scanned here. Such a dynamics has to be associated with the hydration water which remains in liquid state below the transition temperature of bulk-like water, as already seen by DSC for this interfacial layer. In addition, in the case of pristine Si-HPMC hydrogel (blue squares), the amount of water that contributes to the finite NMR signal is approximatively 20 wt % just below the melting point of bulk-like water (0 °C). After the addition of 3 wt% of silica NFs (red squares), the quantity of hydration water inside the hydrogel decreases to ~10 wt% just below 0 °C. These values are also in good agreement with DSC results presented above.

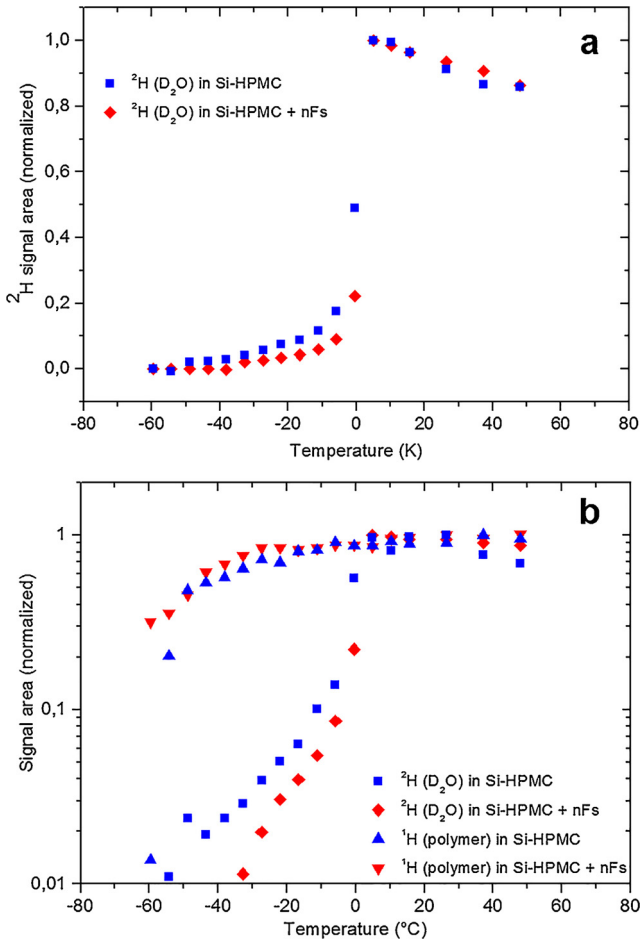

Fig. 3. Normalized signal areas of 2H NMR spectra (a) and 2H and 1H NMR spectra (b) obtained by cryoporometry for pristine Si-HPMC hydrogel (blue squares and up-triangles) and Si-HPMC + 3 wt% NFs hydrogel (red diamonds and down-triangles).

The signal area of ^{2}H atoms (water) increases with increasing temperature up to 7 °C and then stabilizes. At around 0 °C, the abrupt increase of water dynamics for both Si-HPMC (blue) and reinforced Si-HPMC (red) hydrogels can be attributed to the melting of bulk-like water inside the hydrogels, in accordance with DSC results.

Fig. 3b shows the decoupling of polymer's and water's dynamics for both Si-HPMC hydrogels, since the water is deuterated (^{2}H signals represented by squares symbols) and the matrix is protonated (^{1}H signals represented by triangle symbols). Indeed, the dynamics of the polymer (triangles) shows small modification between −40 and + 60 °C: the dynamics of the polymer is quicker than that of confined water at low temperatures for both hydrogel types. However, it is important to point out that such high dynamics is more likely due to the motion of Si-HPMC side chains.

More detailed insight of the dynamics of confined water is given by Pulsed-Gradient Spin-Echo NMR spectroscopy (PGSE). Diffusion coefficients (D) at large space and time scales, *i.e.* at the order of 10 µm and 100 ms, are obtained by this method. The diffusion coefficients of hydrogen atoms in both Si-HPMC based hydrogels were determined at 300 K and were compared to the diffusion coefficient of hydrogen atoms measured in bulk distilled water. All the D values are summarized in Table 1. The diffusion coefficient of bulk distilled water is 2.3(± 0.1) × 10^{-5} cm^2 s^{-1} at 25 °C, in good agreement with values of the literature (Holz, Heil, & Sacco, 2000). The diffusion coefficient of water confined in the pristine Si-HPMC hydrogel is slightly lower (1.9(± 0.1) × 10^{-5} cm^2 s^{-1}), also in very good agreement with the literature (Caccavo et al., 2018). It is important to note that the uncertainty on the diffusion coefficient determination is generally lower than 5%. In other words, at these large space and time scales and at 25 °C, the diffusion of water molecules inside Si-HPMC hydrogel is very similar to that of bulk distilled water. Water molecules in hydrogel thus appear negligibly affected by the presence of polysaccharide pore walls and their mean free path is of the order of 10 µm since this is the space scale probed by this technics. The morphology of the hydrogel, as observed by cryo-SEM that showed micrometer-sized pores, seems to be in accordance with such a mean free path. Even if the cryo-SEM images are subject to caution, as already mentioned above, their consistency with our NMR results is remarkable.

Interestingly, the addition of silica NFs leads to a slight increase of the diffusion coefficient, up to 2.7(± 0.2) × 10^{-5} cm^2 s^{-1}. Therefore, it seems that the presence of silica NFs enhances the diffusion of water molecules throughout the hydrogel ; this could be attributed to a cooperative diffusion of water within the mesoporosity of the NFs. As already mentioned, good mechanical and diffusive properties are important for application of such hydrogels in cartilage and intervertebral disc tissue engineering and the presence of silica NFs by enhancing both of them is thus very interesting.

It is also worth to note that our experiments do not allow us to identify the diffusion process that eventually could be attributed to the dynamics of hydration water. The molecules of hydration water should be bound to the hydrophilic hydrogel matrix by hydrogen bonds and are constantly involved in very fast exchanges between bound-unbound state. Owing to the diffusion time, which was of 50 ms in these experiences, the dynamics of the two water populations (bulk-like and hydration one) are not discernible by the PGSE technique.

4. Conclusions

In summary, Si-HPMC based hydrogels, containing only 2 wt% of polymer, seems to present a highly porous morphology with chemically cross-linked Si-HPMC polymer. Upon addition of 3 wt% of silica nanofibers, a cross-link of the latter occurs with the Si-HPMC polymer leading to a hybrid silica-polymer matrix with enhanced mechanical properties, as shown in our previous study. Each Si-HPMC hydrogel confines two different populations of water, namely "hydration" and "bulk-like water". Hydration water interacts with the hydrophilic hydrogel matrix, with and without NFs. Consequently, its thermodynamical behaviour is modified: hydration water does not show solidification even at very low temperatures (at least until −60 °C). On the other hand, bulk-like water confined within these hydrogels presents a usual solid-to-liquid phase transition at temperature close to 0 °C and its dynamics at room temperature is very similar to that of bulk water. The molecules of bulk-like water can diffuse over micrometric distances throughout Si-HPMC hydrogels without being influenced by the matrix. Such hydrogels appear thus as promising materials for use in tissue

Table 1
Diffusion coefficients of bulk distilled water and water confined within pristine and silica NFs reinforced Si-HPMC hydrogels determined by PGSE at 300 K.

	Distilled water	Si-HPMC hydrogel	Si-HPMC + 3 wt% NFs hydrogel
Diffusion coefficient D [cm^2 s^{-1}]	2.3 (± 0.1) x 10^{-5}	1.9 (± 0.1) x 10^{-5}	2.7 (± 0.2) x 10^{-5}

engineering for cartilage, intervertebral disc or fibrillated heart, both because of possible micro-invasive surgery and because of a sufficiently high water dynamics which is beneficial for the diffusion of nutriments, thus for cell viability.

Acknowledgements

The authors would like to thank Laboratoire de RMN, ICMMO, Université Paris Sud for allowing access to the NMR spectrometers.

References

Adam, M., Bastide, J., Candau, S. J., Cohen Addad, J. P., Joanny, J. F., Lairez, D., ... de Gennes, P. G. (1996). *Physical properties of polymeric gels.* Chichester: John Wiley & Sons Ltd.

Anseth, K. S., Bowman, C. N., & Brannon-Peppas, L. (1996). Mechanical properties of hydrogels and their experimental determination. *Biomaterials, 17*(17), 1647–1657. https://doi.org/10.1016/0142-9612(96)87644-7.

Apkarian, R. P., & Wright, E. R. (2005). Cryo and cryo-etch methods for quality preservation of hydrogels imaged at high magnification by low temperature SEM. *Microscopy and Microanalysis, 11*(Suppl. S02), 1088–1089. https://doi.org/10.1017/S1431927605500163.

Asadi, N., Alizadeh, E., Salehi, R., Khalandi, B., Davaran, S., & Akbarzadeh, A. (2018). Nanocomposite hydrogels for cartilage tissue engineering: A review. *Artificial Cells, Nanomedicine, and Biotechnology, 46*(3), 465–471. https://doi.org/10.1080/21691401.2017.1345924.

Aston, R., Sewell, K., Klein, T., Lawrie, G., & Grøndahl, L. (2016). Evaluation of the impact of freezing preparation techniques on the characterisation of alginate hydrogels by cryo-SEM. *European Polymer Journal, 82*, 1–15. https://doi.org/10.1016/j.eurpolymj.2016.06.025.

Baker, M. J., Denton, T. T., & Herr, C. (2013). An explanation for why it is difficult to form slush nitrogen from liquid nitrogen used previously for this purpose. *Cryobiology, 66*(1), 43–46. https://doi.org/10.1016/j.cryobiol.2012.10.007.

Balagangadharan, K., Dhivya, S., & Selvamurugan, N. (2017). Chitosan based nanofibers in bone tissue engineering. *International Journal of Biological Macromolecules, 104*, 1372–1382. https://doi.org/10.1016/j.ijbiomac.2016.12.046.

Bourges, X., Weiss, P., Daculsi, G., & Legeay, G. (2002). Synthesis and general properties of silated-hydroxypropyl methylcellulose in prospect of biomedical use. *Advances in Colloid and Interface Science, 99*(3), 215–228. https://doi.org/10.1016/S0001-8686(02)00035-0.

Buchtová, N., Réthoré, G., Boyer, C., Guicheux, J., Rambaud, F., Vallé, K., ... Le Bideau, J. (2013). Nanocomposite hydrogels for cartilage tissue engineering: Mesoporous silica nanofibers interlinked with siloxane derived polysaccharide. *Journal of Materials Science: Materials in Medicine, 24*(8), 1875–1884. https://doi.org/10.1007/s10856-013-4951-0.

Caccavo, D., Cascone, S., Lamberti, G., & Barba, A. A. (2018). Hydrogels: experimental characterization and mathematical modelling of their mechanical and diffusive behaviour. *Chemical Society Reviews, 47*(7), 2357–2373. https://doi.org/10.1039/c7cs00638a.

Calvert, P. (2009). Hydrogels for soft machines. *Advanced Materials, 21*(7), 743–756. https://doi.org/10.1002/adma.200800534.

Chau, M., De France, K. J., Kopera, B., Machado, V. R., Rosenfeldt, S., Reyes, L., ... Kumacheva, E. (2016). Composite hydrogels with tunable anisotropic morphologies and mechanical properties. *Chemistry of Materials, 28*(10), 3406–3415. https://doi.org/10.1021/acs.chemmater.6b00792.

Deligkaris, K., Tadele, T. S., Olthuis, W., & van den Berg, A. (2010). Hydrogel-based devices for biomedical applications. *Sensors and Actuators B: Chemical, 147*(2), 765–774. https://doi.org/10.1016/j.snb.2010.03.083.

Drury, J. L., & Mooney, D. J. (2003). Hydrogels for tissue engineering: Scaffold design variables and applications. *Synthesis of Biomimetic Polymers, 24*(24), 4337–4351. https://doi.org/10.1016/S0142-9612(03)00340-5.

Efthymiou, C., Williams, M. A. K., & McGrath, K. M. (2017). Revealing the structure of high-water content biopolymer networks: Diminishing freezing artefacts in cryo-SEM images. *Food Hydrocolloids, 73*, 203–212. https://doi.org/10.1016/j.foodhyd.2017.06.040.

Gaharwar, A. K., Peppas, N. A., & Khademhosseini, A. (2014). Nanocomposite hydrogels for biomedical applications. *Biotechnology and Bioengineering, 111*(3), https://doi.org/10.1002/bit.25160.

Hendrickson, G. R., & Andrew Lyon, L. (2009). Bioresponsive hydrogels for sensing applications. *Soft Matter, 5*(1), 29–35. https://doi.org/10.1039/B811620B.

Henry, N., Clouet, J., Le Bideau, J., Le Visage, C., & Guicheux, J. (2018). Innovative strategies for intervertebral disc regenerative medicine: From cell therapies to multiscale delivery systems. *Biotechnology Advances, 36*(1), 281–294. https://doi.org/10.1016/j.biotechadv.2017.11.009.

Holz, M., Heil, S. R., & Sacco, A. (2000). Temperature-dependent self-diffusion coefficients of water and six selected molecular liquids for calibration in accurate 1H NMR PFG measurements. *Physical Chemistry Chemical Physics, 2*(20), 4740–4742. https://doi.org/10.1039/B005319H.

Jaikumar, D., Sajesh, K. M., Soumya, S., Nimal, T. R., Chennazhi, K. P., Nair, S. V., ... Jayakumar, R. (2015). Injectable alginate-O-carboxymethyl chitosan/nano fibrin composite hydrogels for adipose tissue engineering. *International Journal of Biological Macromolecules, 74*, 318–326. https://doi.org/10.1016/j.ijbiomac.2014.12.037.

Jhon, M. S., & Andrade, J. D. (1973). Water and hydrogels. *Journal of Biomedical Materials Research, 7*(6), 509–522. https://doi.org/10.1002/jbm.820070604.

Lang, Y.-Y., Jiang, T.-Y., Li, S.-M., & Zheng, L.-Y. (2008). Study on physicochemical properties of thermosensitive hydrogels constructed using graft-copolymers of poly (N-isopropylacrylamide) and Guar gum. *Journal of Applied Polymer Science, 108*(6), 3473–3479. https://doi.org/10.1002/app.27948.

Li, X., Cui, Y., Xiao, J., & Liao, L. (2008). Hydrogel–hydrogel composites: The interfacial structure and interaction between water and polymer chains. *Journal of Applied Polymer Science, 108*(6), 3713–3719. https://doi.org/10.1002/app.27854.

Nojoomi, A., Tamjid, E., Simchi, A., Bonakdar, S., & Stroeve, P. (2017). Injectable polyethylene glycol-laponite composite hydrogels as articular cartilage scaffolds with superior mechanical and rheological properties. *International Journal of Polymeric Materials and Polymeric Biomaterials, 66*(3), 105–114. https://doi.org/10.1080/00914037.2016.1182914.

Numata, K., Katashima, T., & Sakai, T. (2011). State of water, molecular structure, and cytotoxicity of silk hydrogels. *Biomacromolecules, 12*(6), 2137–2144. https://doi.org/10.1021/bm200221u.

Ostrowska-Czubenko, J., & Gierszewska-Drużyńska, M. (2009). Effect of ionic crosslinking on the water state in hydrogel chitosan membranes. *Carbohydrate Polymers, 77*(3), 590–598. https://doi.org/10.1016/j.carbpol.2009.01.036.

Petrov, O. V., & Furó, I. (2009). NMR cryoporometry: Principles, applications and potential. *Progress in Nuclear Magnetic Resonance Spectroscopy, 54*(2), 97–122. https://doi.org/10.1016/j.pnmrs.2008.06.001.

Qu, X., Wirsén, A., & Albertsson, A.-C. (2000). Novel pH-sensitive chitosan hydrogels: Swelling behavior and states of water. *Polymer, 41*(12), 4589–4598. https://doi.org/10.1016/S0032-3861(99)00685-0.

Rambaud, F., Vallé, K., Thibaud, S., Julián-López, B., & Sanchez, C. (2009). One-pot synthesis of functional helicoidal hybrid organic–inorganic nanofibers with periodically organized mesoporosity. *Advanced Functional Materials, 19*(18), 2896–2905. https://doi.org/10.1002/adfm.200900431.

Rault, J., Neffati, R., & Judeinstein, P. (2003). Melting of ice in porous glass: Why water and solvents confined in small pores do not crystallize? *The European Physical Journal B - Condensed Matter and Complex Systems, 36*(4), 627–637. https://doi.org/10.1140/epjb/e2004-00017-1.

Sakai, Y., Kuroki, S., & Satoh, M. (2008). Water properties in the super-salt-resistive gel probed by NMR and DSC. *Langmuir, 24*(13), 6981–6987. https://doi.org/10.1021/la800397f.

Sansinena, M., Santos, M. V., Zaritzky, N., & Chirife, J. (2012). Comparison of heat transfer in liquid and slush nitrogen by numerical simulation of cooling rates for French straws used for sperm cryopreservation. *Theriogenology, 77*(8), 1717–1721.

Satarkar, N. S., Biswal, D., & Hilt, J. Z. (2010). Hydrogel nanocomposites: A review of applications as remote controlled biomaterials. *Soft Matter, 6*(11), 2364–2371. https://doi.org/10.1039/B925218P.

Sekine, Y., & Ikeda-Fukazawa, T. (2009). Structural changes of water in a hydrogel during dehydration. *The Journal of Chemical Physics, 130*(3), https://doi.org/10.1063/1.3058616.

Shapiro, J., & Oyen, M. (2013). Hydrogel composite materials for tissue engineering scaffolds. *JOM, 65*(4), 505–516. https://doi.org/10.1007/s11837-013-0575-6.

Slaughter, B. V., Khurshid, S. S., Fisher, O. Z., Khademhosseini, A., & Peppas, N. A. (2009). Hydrogels in regenerative medicine. *Advanced Materials, 21*(32–33), 3307–3329. https://doi.org/10.1002/adma.200802106.

Stejskal, E. O., & Tanner, J. E. (1965). Spin diffusion measurements: Spin echoes in the presence of a time-dependent field gradient. *The Journal of Chemical Physics, 42*(1), 288–292. https://doi.org/10.1063/1.1695690.

Van Vlierberghe, S., Dubruel, P., & Schacht, E. (2011). Biopolymer-based hydrogels as scaffolds for tissue engineering applications: A review. *Biomacromolecules, 12*(5), 1387–1408. https://doi.org/10.1021/bm200083n.

Wichterle, O., & Lim, D. (1960). Hydrophilic gels for biological use. *Nature, 185*(4706), 117–118. https://doi.org/10.1038/185117a0.

Yang, Y., Wang, X., Yang, F., Shen, H., & Wu, D. (2016). A universal soaking strategy to convert composite hydrogels into extremely tough and rapidly recoverable double-network hydrogels. *Advanced Materials, 28*(33), 7178–7184. https://doi.org/10.1002/adma.201601742.

Yoshida, H., Hatakeyama, T., & Hatakeyama, H. (1993). Characterization of water in polysaccharide hydrogels by DSC. *Journal of Thermal Analysis, 40*(2), 483–489. https://doi.org/10.1007/BF02546617.

Yu, P., Bao, R.-Y., Shi, X.-J., Yang, W., & Yang, M.-B. (2017). Self-assembled high-strength hydroxyapatite/graphene oxide/chitosan composite hydrogel for bone tissue engineering. *Carbohydrate Polymers, 155*, 507–515. https://doi.org/10.1016/j.carbpol.2016.09.001.

Zhang, H., Dunphy, D. R., Jiang, X., Meng, H., Sun, B., Tarn, D., ... Brinker, C. J. (2012). Processing pathway dependence of amorphous silica nanoparticle toxicity: Colloidal vs pyrolytic. *Journal of the American Chemical Society, 134*(38), 15790–15804. https://doi.org/10.1021/ja304907c.